Geophysical Research Letters

RESEARCH LETTER
10.1029/2025GL120079

Transient Evolution of Polar Amplification Under Different CO_2 Ramping Rates

Camille Hankel[1,2] and **David B. Bonan**[1,2]

[1]Department of Atmospheric and Climate Science, University of Washington, Seattle, WA, USA, [2]Cooperative Institute for Climate, Ocean, and Ecosystem Studies, University of Washington, Seattle, WA, USA

Key Points:

- The rate of CO_2 increase influences the transient evolution of polar amplification in both hemispheres within a single climate model
- CO_2 increases ≥0.5% yr^{-1} can suppress Arctic amplification for centuries, despite it emerging initially, due to ocean heat transport decline
- Abrupt Antarctic amplification occurs after multiple millennia due to the release of deep ocean heat, with later onset at weaker ramp rates

Supporting Information:

Supporting Information may be found in the online version of this article.

Correspondence to:

C. Hankel,
crhankel@uw.edu

Citation:

Hankel, C., & Bonan, D. B. (2026). Transient evolution of polar amplification under different CO_2 ramping rates. *Geophysical Research Letters*, *53*, e2025GL120079. https://doi.org/10.1029/2025GL120079

Received 21 OCT 2025
Accepted 10 MAR 2026

Abstract Polar amplification is a robust feature of greenhouse-gas-forced climate change. Previous studies have typically examined it over a fixed time period or following an abrupt increase in atmospheric CO_2. Here, we investigate how the transient evolution of polar amplification depends on the rate of atmospheric CO_2 increase up to a fixed concentration using a global climate model. We find that Arctic amplification is initially strong but subsequently suppressed for several centuries when atmospheric CO_2 increases rapidly (≥0.5% yr^{-1}), due to changes in ocean circulation, associated heat transport, and amplifying radiative feedbacks. In contrast, Antarctic amplification emerges gradually across all ramping-rate experiments but exhibits an abrupt increase more than 1,000 years after atmospheric CO_2 stabilizes, triggered by a Ross Sea convective event that transports deep ocean heat to the surface. These findings demonstrate that the rate of forcing strongly shapes how both the magnitude and mechanisms of polar amplification evolve over time.

Plain Language Summary Under increased greenhouse-gas concentrations, Earth's polar regions warm more than the global average, a phenomenon known as polar amplification. Previous studies have examined the causes of polar amplification, typically focusing on specific time periods or abrupt increases in greenhouse gas concentrations. However, it remains unclear how the rate of greenhouse gas increase affects polar amplification. Here, we address this question by analyzing the long-term evolution of polar amplification using a global climate model under several different rates of atmospheric carbon dioxide increase up to the same final concentration. In the Arctic, polar amplification is initially strong, but under rapid carbon-dioxide concentration increases, it temporarily disappears for centuries before re-emerging on millennial timescales due to changes in ocean circulation and heat transport. In the Antarctic, polar amplification emerges gradually across all ramping-rate experiments but exhibits a delayed surge more than 1,000 years after carbon-dioxide concentrations stabilize, linked to the upward transport of deep ocean heat to the surface. These results demonstrate how the same total greenhouse gas concentration change can produce different polar climate responses depending on how quickly the concentrations increase.

1. Introduction

Polar amplification, the phenomenon in which surface temperatures at high latitudes change more than the global average, has been a robust and persistent feature of climate model simulations since the earliest numerical studies of global warming (Manabe & Stouffer, 1980; Manabe & Wetherald, 1975). Observations now confirm this model-predicted signal in the Arctic, which is currently warming at a rate two-to-four times faster than the global average (Chylek et al., 2022; England et al., 2021; Hahn et al., 2021; Rantanen et al., 2022; Screen & Simmonds, 2010; Serreze et al., 2009; Sweeney et al., 2023). By contrast, little to no such amplification has been observed in the Antarctic to date (Hahn et al., 2021).

Numerous mechanisms have been proposed to explain polar amplification (e.g., Holland & Bitz, 2003; Manabe & Stouffer, 1980; Manabe & Wetherald, 1975; Pithan & Mauritsen, 2014; Salzmann, 2017; Stuecker et al., 2018). Surface albedo and temperature feedbacks, which reinforce warming through positive feedback loops, are widely regarded as the primary contributors to Arctic amplification (Hahn et al., 2021; Hall, 2004; Pithan & Mauritsen, 2014; Winton, 2006). Polar amplification, more broadly, has been linked to a moist atmosphere, which enhances poleward energy transport under warming (Armour et al., 2019; Bonan et al., 2018; Feldl & Merlis, 2021; Merlis & Henry, 2018; Roe et al., 2015). The comparatively muted Antarctic amplification has been attributed to both the high surface elevation of the ice sheet (Salzmann, 2017), which produces shallower and less intense climatological temperature inversions and a weaker lapse-rate feedback (Hahn et al., 2020), and ocean

heat uptake, which delays Southern Ocean warming (Armour et al., 2016). However, many of these mechanisms for polar amplification are based on analyses of specific time periods (e.g., Pithan & Mauritsen, 2014), which may limit our understanding of the underlying causes and transient nature of polar amplification. For example, on long timescales, the processes that currently suppress Antarctic warming, such as deep ocean heat uptake, are expected to weaken, potentially leading to greater Antarctic warming in the future (Armour et al., 2016; Danabasoglu & Gent, 2009; Hill et al., 2022; Marshall et al., 2015).

Recent work has begun to examine the transient evolution of polar amplification, from its rapid onset within just a few years (Janoski et al., 2023; Previdi et al., 2020) to its development over centennial and millennial timescales (Armour et al., 2013; Hill et al., 2022; Holland & Landrum, 2021; Kay et al., 2024). These studies suggest that different mechanisms dominate at different stages of the climate response to radiative forcing. Distinct mechanisms for Arctic amplification have also been identified by examining how the climate responds to different levels of greenhouse gas forcing, highlighting possible nonlinearities in the system (e.g., Liang et al., 2022). In contrast, less attention has been given to the role of the rate of increase of atmospheric carbon-dioxide (CO_2) in shaping the polar climate response, despite previous work showing its importance for other large-scale climate processes such as the Atlantic meridional overturning circulation (AMOC, Hankel, 2025b; Stocker & Schmittner, 1997), the carbon cycle (Krasting et al., 2014), and the global mean surface temperature (Stouffer & Manabe, 1999). This represents a potentially important gap, as the growth rate of atmospheric CO_2 has varied under anthropogenic emissions, ranging from about 0.2% yr^{-1} in the early 1960s to 0.6% yr^{-1} in the 2000s (Figure S1 in Supporting Information S1). Although future emissions scenarios project a slowing of this rate (Figure S2 in Supporting Information S1), the legacy of past and near-term ramping rates may have long-lasting impacts on polar climate processes. This raises a key question: does the rate of atmospheric CO_2 increase influence polar amplification?

In this study, we use a comprehensive climate model to investigate how the rate of atmospheric CO_2 increase influences the evolution of polar amplification over multiple millennia. We find that the trajectory of polar amplification in each hemisphere is influenced by the atmospheric CO_2 ramping rate. Initially, the Arctic exhibits strong warming amplification; however, in simulations with the fastest ramping rates ($\geq$0.5% yr^{-1}), Arctic amplification is subsequently suppressed for several centuries before re-emerging nearly 1,000 years later. By contrast, Antarctic amplification is initially strongest under the fastest ramping rates, yet all simulations display an abrupt increase approximately 1,000–2,000 years into the simulations. At quasi-equilibrium, all ramping scenarios eventually converge to similar amplification factors for a given hemisphere. Using a diagnostic feedback-forcing framework, we link these responses to specific physical mechanisms. The suppression of Arctic amplification for several centuries arises from a decline in poleward ocean heat transport associated with the AMOC weakening and an expansion of sea ice, which leads to regional cooling. The abrupt increase in Antarctic amplification is driven by enhanced ocean heat transport and sudden sea ice loss, triggered by the gradual development of a salinity anomaly that de-stratifies the Ross Sea and initiates deep convection. These findings highlight that the rate of atmospheric CO_2 increase can play a key role in shaping the transient evolution of polar amplification in both hemispheres.

2. Materials and Methods

2.1. Climate Model Simulations

The climate model simulations were originally conducted by Hankel (2025b) using the Community Earth System Model version 1.2.2.1 with a T31_g37 grid, which corresponds to a nominal horizontal resolution of 3° in the ocean and 3.5° in the atmosphere (Shields et al., 2012). The atmospheric model is CAM4 with 26 vertical levels, and the ocean model is POP2 with 60 vertical levels. Low horizontal resolution introduces some mean-state biases (Shields et al., 2012): Arctic sea ice is overly extensive, including in the North Atlantic region, while Antarctic sea ice is also high but remains within the CMIP6 range (Figure S3 in Supporting Information S1). The Arctic bias likely reflects weaker northward ocean heat transport in the Atlantic, consistent with a mean-state AMOC at 26.5°N that is weaker than RAPID observations (Cunningham et al., 2007).

The CO_2 ramping simulations were initialized from the end of a 2,500-year preindustrial control run in which atmospheric CO_2 was fixed at 284.7 ppm. From this initial state, atmospheric CO_2 was increased at seven different rates, ranging from 0.0625% yr^{-1} to 4% yr^{-1}, until it reached twice the preindustrial concentration (hereafter '2 $\times$ CO_2', 569.4 ppm). After 2 $\times$ CO_2, the atmospheric CO_2 was held constant for several hundred

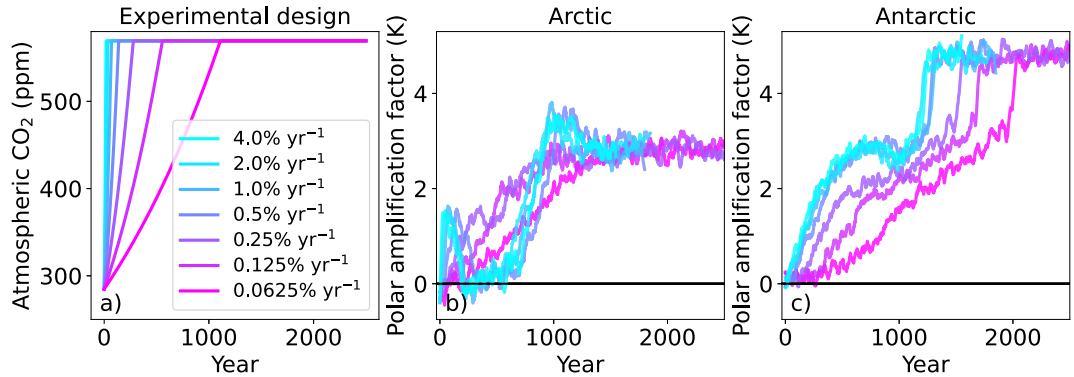

Figure 1. Panel (a) shows the time evolution of atmospheric CO_2 concentration in the seven different CO_2 ramping-rate simulations. Panels (b, c) show the polar amplification factor in the Arctic (60°N–90°N) and the Antarctic (60°S–90°S), respectively, across all seven CO_2 ramping-rate experiments. The polar amplification factor is defined as the difference between the annual-mean surface temperature anomaly of the Arctic or Antarctic and the global mean. All time series have been smoothed using a 30-year linear filter.

additional years until the simulations approached quasi-equilibrium, defined as near-zero global-mean net top-of-atmosphere radiation anomalies. This resulted in different total simulation lengths across the ramping experiments. The experimental design is illustrated in Figure 1a.

2.2. Feedback-Forcing Framework

To understand the mechanisms contributing to the transient evolution of polar amplification in each simulation, we examine changes in the local atmospheric energy budget (Crook et al., 2011; Feldl et al., 2017; Goosse et al., 2018; Hahn et al., 2021; Pithan & Mauritsen, 2014) and decompose the changes in surface temperature (skin temperature, ΔT) into partial temperature contributions from the effective radiative forcing ($\mathcal{F}$), radiative feedbacks (λ), ocean heat uptake (OHU), and change in atmospheric heat flux convergence ($\Delta(\nabla \cdot \mathrm{AHT})$), yielding

$$\Delta T = -\frac{1}{\overline{\lambda_P}}\left(\mathcal{F} + \left(\lambda_P' + \sum_i \lambda_i\right)\Delta T + \mathrm{OHU} - \Delta(\nabla \cdot \mathrm{AHT}) + \epsilon\right), \quad (1)$$

where $\overline{\lambda_P}$ is the global- and annual-mean Planck feedback, λ_P' is the deviation of the local Planck feedback from $\overline{\lambda_P}$, λ_i represents the remaining radiative feedbacks (water vapor, cloud, surface albedo, and lapse rate), and ϵ is a residual term.

To calculate each term in Equation 1, anomalies in the time series of the variables in the CO_2 ramping experiments are defined relative to the mean over the final 30 years of the preindustrial control simulation. Following Soden et al. (2008) and Shell et al. (2008), we use radiative kernels to estimate individual radiative feedbacks contributing to λ. Specifically, we use the CAM5 radiative kernel (Pendergrass et al., 2018) via the Climkern python package (Janoski et al., 2024), which provides built-in functions for calculating radiative feedbacks. To estimate the time-evolving all-sky effective radiative forcing, $\mathcal{F}$, we calculate the time-evolving clear-sky effective radiative forcing in each experiment as the total (longwave plus shortwave) clear-sky top-of-atmosphere (TOA) net radiation anomaly minus the TOA contributions of all clear-sky feedbacks, and estimate $\mathcal{F}$ as the clear-sky effective radiative forcing divided by 1.16 (Hahn et al., 2021; Soden et al., 2008).

The term $\Delta(\nabla \cdot \mathrm{AHT})$ is calculated as the difference between annual-mean anomalies in net TOA energy fluxes minus the net surface energy fluxes. The term OHU is calculated as the change in net surface energy fluxes, with positive defined upward (indicating energy release from the ocean to the atmosphere). We further partition OHU into separate contributions from ocean heat transport convergence (OHT) and storage (OHS). The OHT term is calculated using the model output "NHEAT" variable, which reports the total vertically integrated ocean heat transport at each latitude. We use values at the grid points closest to 60°S and 60°N, normalized by the area poleward of 60°. The OHS term is calculated as the difference between the OHU and OHT terms.

3. Results

We begin by quantifying the magnitude of polar amplification in both hemispheres across the seven atmospheric CO_2 ramping rate experiments (Figure 1). To avoid dividing by near-zero values, the polar amplification factor is defined as the difference between the surface temperature anomaly in the polar regions (60°–90°N and 60°–90°S) and the global-mean surface temperature anomaly (Huo et al., 2024). This metric, previously used to study short-term polar amplification (Francis & Vavrus, 2015; Janoski et al., 2023), takes positive values when the poles warm more than the global mean. Figure S4 in Supporting Information S1 shows the temporal evolution of the zonal-mean surface temperature anomaly across the experiments.

All ramping rate experiments exhibit polar amplification in both hemispheres, but the timing and magnitude vary, with Antarctic amplification lagging that of the Arctic amplification by several hundred years (Figures 1b and 1c). In the more rapid CO_2 ramping experiments ($\geq$0.5% yr^{-1}), Arctic warming is transiently suppressed between years 250 and 750, corresponding to a near disappearance of Arctic amplification that persists for several centuries (Figure 1b). When Arctic amplification re-emerges, it is followed by a period of "overshoot," during which the polar amplification factor temporarily exceeds its final equilibrium value. By contrast, in the slower CO_2 ramping experiments (<0.5% yr^{-1}), Arctic amplification does not exhibit transient suppression and instead increases relatively monotonically (Figure 1b).

In the Southern Hemisphere, the polar amplification factor generally increases more rapidly in experiments with faster CO_2 ramping, with more rapid CO_2 increases producing earlier Antarctic amplification. Interestingly, all simulations show a sharp rise in the amplification factor due to abrupt Antarctic warming (characterized by maximum rates of warming ranging from 1.56 to 2.25 K/decade, Figure 1c). This pronounced warming occurs between approximately 60°S and 80°S, more than 1,000 years after CO_2 concentrations stop increasing (Figure S4 in Supporting Information S1). While the magnitude of this abrupt warming is largely independent of the ramping rate, its timing varies: in the 4% yr^{-1} experiment it occurs around year 1,250, whereas in the 0.0625% yr^{-1} experiment it occurs around year 2,000 (Figure 1c).

3.1. Mechanisms of the Transient Evolution of Polar Amplification

To understand the mechanisms responsible for the transient evolution of polar amplification in both hemispheres, we decompose the changes in surface temperature into partial temperature contributions via a diagnostic forcing-feedback framework (see Section 2.2). We analyze four time periods spanning the transient disappearance of Arctic amplification and the subsequent abrupt increase in Antarctic amplification, and show results for every other CO_2 ramping rate simulation (4% yr^{-1}, 1% yr^{-1}, 0.25% yr^{-1}, and 0.0625% yr^{-1}) to capture the range of behaviors across the ramping rate experiments.

3.1.1. Arctic Amplification

Figure 2 shows the contribution of each mechanism in Equation 1 to Arctic versus global warming. Dots above the dashed 1× line indicate processes that contribute to Arctic amplification. The residual between the sum of the partial temperature contributions (all colored dots) and the total surface temperature change is displayed in the top panel (white dots). The total surface temperature change in the top row of Figure 2 (black dots) illustrates the ramping-rate-dependent transient disappearance of Arctic amplification. In the 4% yr^{-1} and 1% yr^{-1} ramping-rate experiments, Arctic warming declines from about 2× to 1× the global mean between years 100 and 300 (moving from the smallest to next-largest black dot), whereas in the 0.25% yr^{-1} and 0.0625% yr^{-1} ramping-rate experiments, Arctic warming remains roughly 2× the global-mean warming throughout the entirety of the simulation. The next row shows the contribution of ocean heat uptake (OHU), decomposed into contributions from ocean heat storage (OHS) and transport (OHT). A key factor causing suppressed Arctic amplification around year 300 in the faster ramping experiments is Arctic cooling from ocean heat uptake, which is driven primarily by reduced ocean heat transport rather than changes in ocean heat storage (compare blue and orange dots, Figure 2). The 0.25% yr^{-1} experiment exhibits a weaker signal of this transient reduction in ocean heat transport, suggesting that the suite of CO_2 ramping experiments represents a continuum of oceanic behaviors.

The middle row of Figure 2 shows the partial temperature contributions of the surface albedo (α), lapse rate (LR), and Planck (P') feedbacks, which all covary with and are closely tied to Arctic sea ice (e.g., Feldl et al., 2020). All three feedbacks cause less Arctic warming in year 300 compared to year 100 in the rapid CO_2 ramping

10.1029/2025GL120079

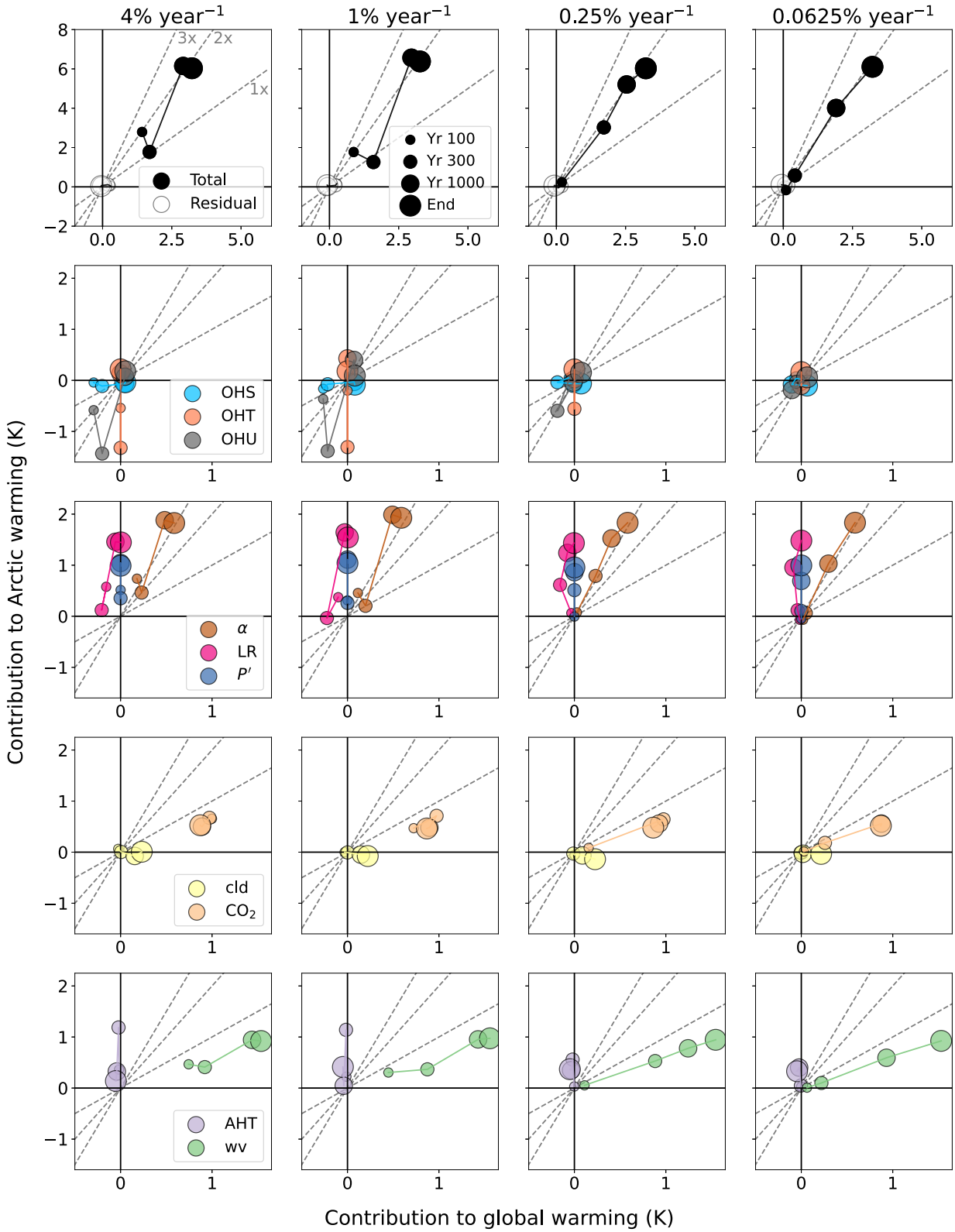

Figure 2. Contribution of different mechanisms to Arctic-versus global-mean surface temperature change for four of the seven CO_2 ramping-rate experiments, as indicated in the column titles. For each mechanism, four dots represent 30-year time-averages centered on year 100, year 300, year 1,000, and 15 years before the end of each simulation. Dot size increases with time, as indicated by the legend. The light gray dashed lines denote slopes (indicated by the labels) that correspond to different amplification factors as defined by another common metric (Arctic warming divided by global mean warming) for comparison.

experiments, consistent with a modest expansion of sea ice area that occurs in response to the decline in OHT over the same period (Figure S12 in Supporting Information S1). For example, at year 100 in the 4% y^{-1} experiment, the surface albedo feedback causes about 3× as much Arctic warming compared to the global mean but declines to about 2× by year 300 (Figure 2).

The bottom two rows of Figure 2 show partial temperature contributions from the net shortwave and longwave cloud (cld) and water vapor (wv) feedbacks, changes in atmospheric heat flux convergence, and the effective radiative forcing from CO_2 changes. The cloud feedback and CO_2 forcing contribute little to the rate-dependent transient suppression of Arctic amplification, instead evolving in a nearly linear, monotonic manner and lying close to the 1× line in all experiments (with a small cancellation between the cloud shortwave and longwave components). The water vapor feedback makes only a minor contribution to suppressed Arctic amplification, consistent with a transient Arctic cooling that reduces specific humidity around year 300 in the rapid CO_2 ramping experiments. Notably, changes in atmospheric heat flux convergence contribute to around 1 K of Arctic warming between years 100 and 300 in the fast-ramping experiments, which would *enhance* Arctic amplification; we interpret this as an atmospheric response to the surface cooling induced by a reduction of ocean heat transport into the region.

The large contribution of ocean heat transport to the transient suppression of Arctic amplification suggests a role for ocean circulation changes and potentially the Atlantic Meridional Overturning Circulation (AMOC), which is a dominant contributor to ocean heat transport in the Atlantic basin. Hankel (2025b) showed that the AMOC weakens substantially more under rapid CO_2 increases than under gradual ones, and that the reduction of northward heat transport per unit AMOC decline is also greater in the more rapid CO_2 increase scenarios.

To test whether the rate-dependent AMOC weakening is indeed related to the suppression of Arctic amplification, Figure S5 in Supporting Information S1 shows the spatial patterns of each mechanism in Equation 1 for the most rapid CO_2 ramping experiment during the time period of Arctic amplification suppression. Around year 300, the main region of Arctic cooling is centered over the North Atlantic and Nordic Seas, where the AMOC terminates. In this region, the same mechanisms identified in Figure 2 as drivers of transient Arctic cooling—ocean heat uptake, lapse rate, and albedo feedbacks—also show strong negative contributions, indicating that the AMOC decline is likely a shared underlying cause. By the end of the simulation, when Arctic amplification re-emerges, this North Atlantic cooling signature disappears, and both the lapse rate and surface albedo feedbacks switch to positive warming contributions, consistent with the AMOC having fully recovered to its preindustrial strength (Figure S9 in Supporting Information S1).

In contrast, the more gradual CO_2 ramping experiments do not exhibit such regionally coherent cooling signals at any time (not shown); instead, Arctic amplification and the mechanisms that contribute to it emerge more smoothly in time. Figure S9 in Supporting Information S1 further shows the time series of ocean heat transport into the Arctic alongside the AMOC strength for all the CO_2 ramping experiments, highlighting their close temporal coherence. Taken together, these results strongly support the interpretation that greater AMOC weakening under the faster CO_2 ramping rates suppresses Arctic amplification—both directly through reduced ocean heat transport into the Arctic and indirectly through its influence on Arctic sea ice-related radiative feedbacks that further enhance regional cooling (Figure S5 in Supporting Information S1). The latter mechanism is key for understanding why the slower ramping-rate experiments show little-to-no suppression of Arctic amplification despite still undergoing some AMOC weakening: in these experiments, the decline in ocean heat transport into the Arctic is not great enough to induce sea ice re-growth and associated radiative feedbacks that would further enhance the regional cooling (Figure S7 in Supporting Information S1). In other words, not only does the AMOC and associated poleward OHT weaken by less under more gradual CO_2 ramping rates, but the sensitivity of Arctic temperatures to the AMOC decline is also less due to the lack of response from other feedbacks.

3.1.2. Antarctic Amplification

Figure 3 shows the contribution of each mechanism in Equation 1 to Antarctic versus global warming. We focus primarily on the changes between year 1,000 and the end of the simulations (the two largest dots in all panels),

10.1029/2025GL120079

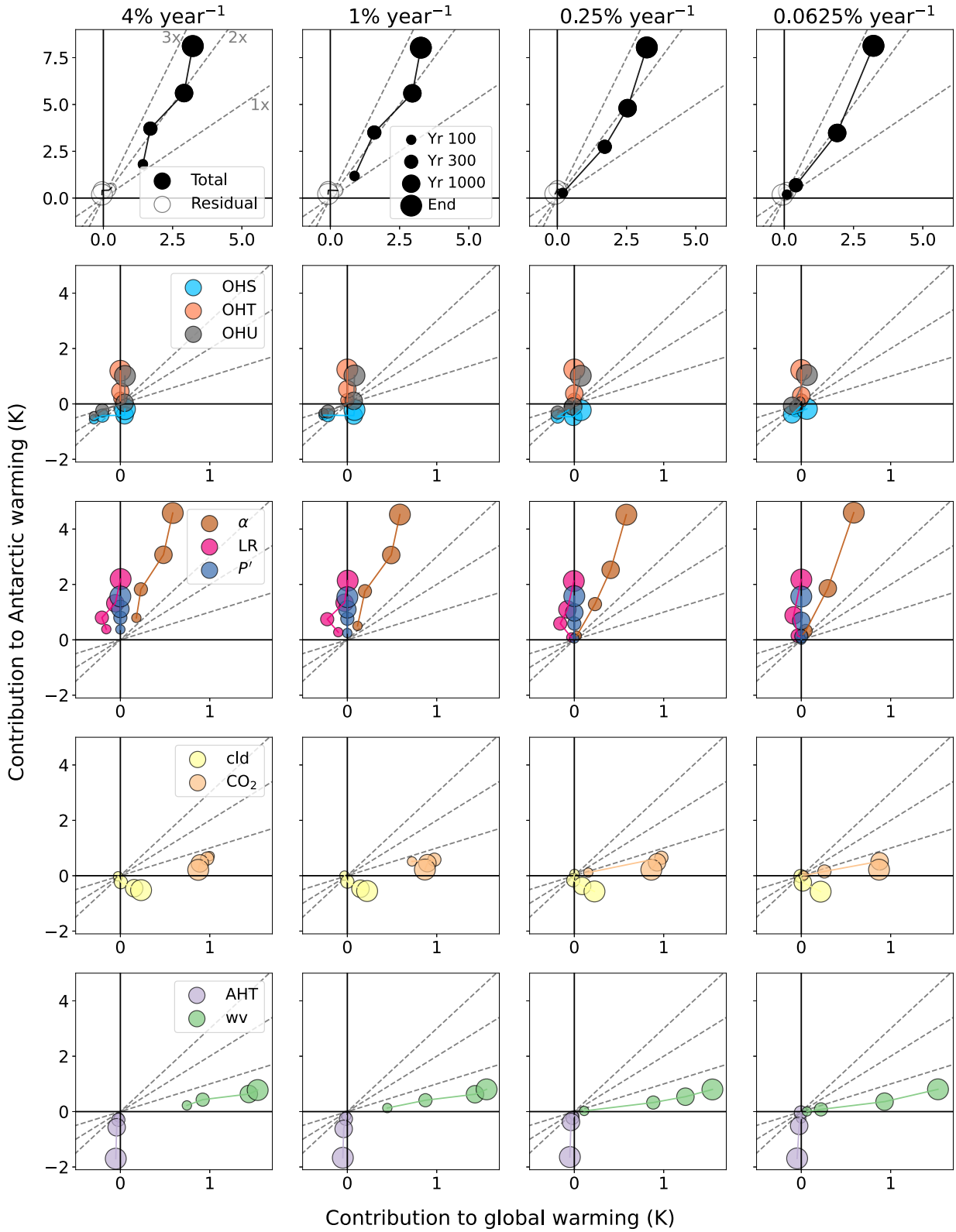

Figure 3. Same as Figure 2, but with contributions to surface temperature change in the Antarctic (60°S–90°S) on the *y*-axis.

during which Antarctic warming increases abruptly from 2× to nearly 3× the global-mean in all simulations, albeit at different times (Figure 3, top row).

In the middle row of Figure 3, the surface albedo feedback emerges as the dominant contributor to this abrupt Antarctic warming, with the lapse rate and Planck feedbacks contributing modest amounts. The involvement of all three feedbacks indicates significant Antarctic sea ice changes occur during this period, which is confirmed by Figure S13 in Supporting Information S1 showing an abrupt sea ice retreat in all experiments late in the simulations. The second row of Figure 3 further shows that ocean heat uptake, driven primarily by an increase in ocean heat transport, also contributes to approximately 1 K of Antarctic warming during this period.

It is striking that such large and rapid changes in Antarctic sea ice occur more than 1,000 years after CO_2 concentrations stabilize, while the rest of the global climate is relatively stable. This suggests a role for long-timescale ocean processes. Figure S6 in Supporting Information S1 shows the spatial pattern of surface temperature change implied by each mechanism in Equation 1 over the Antarctic for the most rapid CO_2 ramping experiment, comparing year 1,000 (before the abrupt warming) to the end of the simulation. The Ross Sea (highlighted in green) emerges as the region with the largest increase in warming over this period. In this region, ocean heat uptake and a positive surface albedo feedback contribute approximately equally to the warming after year 1,000. Atmospheric heat convergence leads to a large, counteracting cooling signal in this region; we interpret this as an atmospheric response to the local surface warming.

To assess whether ocean processes drive the abrupt sea ice loss in the Ross Sea, Figure S10 in Supporting Information S1 shows the full-column changes in ocean potential density, potential temperature, and absolute salinity averaged over the Ross Sea for both the fastest and slowest CO_2 ramping experiments. Figures S10b and S10e in Supporting Information S1 show that the late-stage Ross Sea warming is characterized by the sudden upward flux of heat toward the surface, which is consistent with a large-scale convective event. Figures S10c and S10f in Supporting Information S1 show a slow reduction in subsurface density stratification leading up to this event. While the water column generally becomes lighter over the course of the simulations from warming and freshening, the intermediate waters start to become heavier during the 400 years preceding the convective event due to a gradual salinification in the upper 1,000 m, which ultimately destratifies the water column (Figures S10a, S10d, and S11 in Supporting Information S1). We note that the region from 0 to 60°E also exhibits rapid warming in all experiments (of a smaller magnitude than in the Ross Sea) that contributes to the surge in Antarctic amplification. Interestingly, we find that this warming also coincides with a local ocean convective event preceded by gradual subsurface salinity changes, suggesting a common driver between the two regions.

In summary, the sudden increase in Antarctic amplification, which occurs more than 1,000 years after CO_2 stabilization, is primarily caused by rapid sea ice loss and enhanced surface warming in the Ross Sea driven by both ocean heat uptake changes and the surface albedo feedback. The abrupt sea ice loss coincides with an apparent convective event that brings warmer waters from depth to the surface. The fact that this convective event is preconditioned by centuries of gradual upper-ocean salinification suggests it is a driver of, rather than a response to, the rapid sea ice loss.

4. Discussion and Conclusions

Polar amplification is a prominent feature of modern-day climate change, yet its dependence on the rate of atmospheric CO_2 increase was previously unexplored. In this study, we examined the long-term evolution of polar amplification in a set of global climate model simulations in which the rate of atmospheric CO_2 increase up to $2 \times CO_2$ varied. We found that under rapid rates of CO_2 increase ($\geq 0.5\%$ year^{-1}), Arctic amplification was initially strong but then disappeared for several centuries, while under more gradual CO_2 increases it emerged smoothly and increased monotonically. The suppression of Arctic amplification in the rapid CO_2 ramping rate experiments was due to the greater weakening of the AMOC, which led to a transient period of Arctic cooling via reduced northward ocean heat transport, Arctic sea ice re-growth, and negative surface albedo and lapse-rate feedbacks.

In the Antarctic, all simulations exhibited an abrupt increase in polar amplification more than 1,000 years after CO_2 stops increasing, albeit at different times, with a more delayed abrupt increase under slower CO_2 ramping rates. This abrupt increase was linked to a convective event in the Ross Sea that drove the upward flux of oceanic heat and a sudden loss of sea ice. We found that the convective event was triggered by salinity, which gradually

increased in the upper ocean of the Ross Sea. While it would be difficult to conclusively establish the cause of the increasing upper-ocean salinity that precipitates the convective events and sea ice loss, we note that the net freshwater flux at the surface over the Ross Sea is increasing throughout this period (likely due to an enhanced hydrological cycle and reduced sea ice production), and therefore does not explain the increasing salinity. We therefore hypothesize that the salinification is due to either a reduction in Antarctic Bottom Water production that typically exports salinity from the upper ocean to the abyss (e.g., Chen et al., 2023; De Lavergne et al., 2014) or internal ocean processes, such as a change in the interbasin salinity exchange (i.e., incoming North Atlantic Deep Water). The long timescales of the salinity anomalies suggest they could also be linked to AMOC-driven interhemispheric coupling (e.g., Pedro et al., 2018), although the similar convective response across experiments with differing levels of AMOC weakening implies this mechanism may not be dominant.

It is important to note that our analysis is based on a single, coarse-resolution climate model (CESM1.2.2.1; Shields et al., 2012). To assess the generalizability of our results, we examine LongRunMIP climate model simulations ranging from a nominal resolution of 1°–2° (Rugenstein et al., 2019) forced by an instantaneous doubling of CO_2. Two models (HadCM3L and CCSM3) exhibit a transient reduction in Arctic amplification within the first century, one model (CESM1.0.4) displays large multi-centennial oscillations in Arctic amplification, which coincide with AMOC oscillations, and the other two models (CNRM-CM6-1 and MPI-ESM1.2) exhibit no clear signal of suppressed Arctic amplification (Figure S14 in Supporting Information S1). Our simulation is the only one out of the six models that shows a complete disappearance of Arctic amplification; this may be because of its overly extensive sea ice in the North Atlantic, which makes the sea ice and related feedbacks more sensitive to the weakening AMOC. Nonetheless, recent studies have also linked weaker Arctic amplification to AMOC weakening in other climate models at higher resolutions and higher CO_2 levels (Liang et al., 2022; Mitevski et al., 2021), and found different levels of Arctic amplification in simulations with strong versus weak AMOC slowdowns (Lee et al., 2024), suggesting that the mechanism identified here may operate across climate models and forcing scenarios.

For the Antarctic, none of the LongRunMIP models exhibit an abrupt increase in polar amplification (Figure S15 in Supporting Information S1); however, three of the five models (HadCM3L, CNRM-CM6.1, MPI-ESM1.2) do not simulate beyond 1,000 years, which may be too short to capture the convective events seen in our simulations. None of these models (including the one used in this study) includes resolved ocean eddies or increasing meltwater from a retreating Antarctic ice sheet, which would also likely influence such convective events both by supplying additional surface freshwater and by altering bottom water production. Note that other types of convective events have been reported in both observations and climate models elsewhere in the Southern Ocean, such as the Weddell Sea (Gordon, 2014; Pedro et al., 2016), motivating further investigation into the long-term behavior of deep convection in the Southern Ocean.

Overall, these results demonstrate that both the magnitude and mechanisms of polar amplification depend strongly on the rate of CO_2 increase, suggesting that policies may need to target not only the amount, but also the rate of future emissions. Notably, the observed historical growth rate of atmospheric CO_2 (0.2%–0.6% yr^{-1}) falls within the range where Arctic amplification is suppressed based on our simulations, raising questions about how the legacy of past emissions will impact the evolution of Earth's polar regions for centuries to come. While this study uses a single, low-resolution climate model with known mean-state biases, the results highlight the need for a robust understanding of rate-dependent climate responses and motivate further investigation of the impacts of slower or faster CO_2 growth rates on other processes and across other climate models.

Conflict of Interest

The authors declare no conflicts of interest relevant to this study.

Availability Statement

All underlying climate model output data used to generate the figures are available at Zenodo (Hankel, 2025a). Observed CO_2 concentrations used in Figure S1 of Supporting Information S1 can be found at https://gml.noaa.gov/ccgg/trends/, and all CMIP6 data used in the Supporting Information S1 can be accessed via https://aims2.llnl.gov/search.

Acknowledgments
CH and DB were supported by CICOES Postdoctoral Fellowships. CH was also supported by NSF award AGS-PRF-2414916. The climate model simulations were performed using resources from the National Center for Atmospheric Research Exploratory Computing Allocation number UHAR0020 awarded to CH. This publication is partially funded by CICOES under NOAA Cooperative Agreement NA20OAR4320271, contribution No. 2025-1499. The authors thank two anonymous reviewers and the Editor for their careful and constructive feedback, which improved the analysis in this manuscript.

References

Armour, K. C., Bitz, C. M., & Roe, G. H. (2013). Time-varying climate sensitivity from regional feedbacks. *Journal of Climate*, *26*(13), 4518–4534. https://doi.org/10.1175/jcli-d-12-00544.1

Armour, K. C., Marshall, J., Scott, J. R., Donohoe, A., & Newsom, E. R. (2016). Southern ocean warming delayed by circumpolar upwelling and equatorward transport. *Nature Geoscience*, *9*(7), 549–554. https://doi.org/10.1038/ngeo2731

Armour, K. C., Siler, N., Donohoe, A., & Roe, G. H. (2019). Meridional atmospheric heat transport constrained by energetics and mediated by large-scale diffusion. *Journal of Climate*, *32*(12), 3655–3680. https://doi.org/10.1175/jcli-d-18-0563.1

Bonan, D. B., Armour, K., Roe, G., Siler, N., & Feldl, N. (2018). Sources of uncertainty in the meridional pattern of climate change. *Geophysical Research Letters*, *45*(17), 9131–9140. https://doi.org/10.1029/2018gl079429

Chen, J.-J., Swart, N. C., Beadling, R., Cheng, X., Hattermann, T., Jüling, A., et al. (2023). Reduced deep convection and bottom water formation due to Antarctic meltwater in a multi-model ensemble. *Geophysical Research Letters*, *50*(24), e2023GL106492. https://doi.org/10.1029/2023gl106492

Chylek, P., Folland, C., Klett, J. D., Wang, M., Hengartner, N., Lesins, G., & Dubey, M. K. (2022). Annual mean arctic amplification 1970–2020: Observed and simulated by CMIP6 climate models. *Geophysical Research Letters*, *49*(13), e2022GL099371. https://doi.org/10.1029/2022gl099371

Crook, J. A., Forster, P. M., & Stuber, N. (2011). Spatial patterns of modeled climate feedback and contributions to temperature response and polar amplification. *Journal of Climate*, *24*(14), 3575–3592. https://doi.org/10.1175/2011jcli3863.1

Cunningham, S. A., Kanzow, T., Rayner, D., Baringer, M. O., Johns, W. E., Marotzke, J., et al. (2007). Temporal variability of the Atlantic meridional overturning circulation at 26.5 n. *Science*, *317*(5840), 935–938. https://doi.org/10.1126/science.1141304

Danabasoglu, G., & Gent, P. R. (2009). Equilibrium climate sensitivity: Is it accurate to use a slab ocean model? *Journal of Climate*, *22*(9), 2494–2499. https://doi.org/10.1175/2008jcli2596.1

De Lavergne, C., Palter, J. B., Galbraith, E. D., Bernardello, R., & Marinov, I. (2014). Cessation of deep convection in the open southern ocean under anthropogenic climate change. *Nature Climate Change*, *4*(4), 278–282. https://doi.org/10.1038/nclimate2132

England, M. R., Eisenman, I., Lutsko, N. J., & Wagner, T. J. (2021). The recent emergence of arctic amplification. *Geophysical Research Letters*, *48*(15), e2021GL094086. https://doi.org/10.1029/2021gl094086

Feldl, N., Bordoni, S., & Merlis, T. M. (2017). Coupled high-latitude climate feedbacks and their impact on atmospheric heat transport. *Journal of Climate*, *30*(1), 189–201. https://doi.org/10.1175/jcli-d-16-0324.1

Feldl, N., & Merlis, T. M. (2021). Polar amplification in idealized climates: The role of ice, moisture, and seasons. *Geophysical Research Letters*, *48*(17), e2021GL094130. https://doi.org/10.1029/2021gl094130

Feldl, N., Po-Chedley, S., Singh, H. K., Hay, S., & Kushner, P. J. (2020). Sea ice and atmospheric circulation shape the high-latitude lapse rate feedback. *npj Climate and Atmospheric Science*, *3*(1), 41. https://doi.org/10.1038/s41612-020-00146-7

Francis, J. A., & Vavrus, S. J. (2015). Evidence for a wavier jet stream in response to rapid arctic warming. *Environmental Research Letters*, *10*(1), 014005. https://doi.org/10.1088/1748-9326/10/1/014005

Goosse, H., Kay, J. E., Armour, K. C., Bodas-Salcedo, A., Chepfer, H., Docquier, D., et al. (2018). Quantifying climate feedbacks in Polar Regions. *Nature Communications*, *9*(1), 1919. https://doi.org/10.1038/s41467-018-04173-0

Gordon, A. L. (2014). Southern ocean polynya. *Nature Climate Change*, *4*(4), 249–250. https://doi.org/10.1038/nclimate2179

Hahn, L. C., Armour, K. C., Battisti, D. S., Donohoe, A., Pauling, A., & Bitz, C. M. (2020). Antarctic elevation drives hemispheric asymmetry in polar lapse rate climatology and feedback. *Geophysical Research Letters*, *47*(16), e2020GL088965. https://doi.org/10.1029/2020gl088965

Hahn, L. C., Armour, K. C., Zelinka, M. D., Bitz, C. M., & Donohoe, A. (2021). Contributions to polar amplification in CMIP5 and CMIP6 models. *Frontiers in Earth Science*, *9*, 710036. https://doi.org/10.3389/feart.2021.710036

Hall, A. (2004). The role of surface albedo feedback in climate. *Journal of Climate*, *17*(7), 1550–1568. https://doi.org/10.1175/1520-0442(2004)017<1550:trosaf>2.0.co;2

Hankel, C. (2025a). Data for "Transient evolution of polar amplification under different CO_2 ramping rates" [Dataset]. https://doi.org/10.5281/zenodo.17389320

Hankel, C. (2025b). The effect of CO_2 ramping rate on the transient weakening of the Atlantic meridional overturning circulation. *Proceedings of the National Academy of Sciences*, *122*(1), e2411357121. https://doi.org/10.1073/pnas.2411357121

Hill, S. A., Burls, N. J., Fedorov, A., & Merlis, T. M. (2022). Symmetric and antisymmetric components of polar-amplified warming. *Journal of Climate*, *35*(20), 6757–6772. https://doi.org/10.1175/jcli-d-20-0972.1

Holland, M. M., & Bitz, C. M. (2003). Polar amplification of climate change in coupled models. *Climate Dynamics*, *21*(3), 221–232. https://doi.org/10.1007/s00382-003-0332-6

Holland, M. M., & Landrum, L. (2021). The emergence and transient nature of arctic amplification in coupled climate models. *Frontiers in Earth Science*, *9*, 719024. https://doi.org/10.3389/feart.2021.719024

Huo, Y., Wang, H., Lu, J., Fu, Q., Jonko, A. K., Lee, Y. J., et al. (2024). Assessing radiative feedbacks and their contribution to the arctic amplification measured by various metrics. *Journal of Geophysical Research: Atmospheres*, *129*(21), e2024JD040880. https://doi.org/10.1029/2024jd040880

Janoski, T. P., Mitevski, I., Kramer, R. J., Previdi, M., & Polvani, L. M. (2024). Climkern v1. 1.2: A new python package and kernel repository for calculating radiative feedbacks. *EGUsphere*, *2024*, 1–23.

Janoski, T. P., Previdi, M., Chiodo, G., Smith, K. L., & Polvani, L. M. (2023). Ultrafast arctic amplification and its governing mechanisms. *Environmental Research: Climate*, *2*(3), 035009. https://doi.org/10.1088/2752-5295/ace211

Kay, J. E., Liang, Y.-C., Zhou, S.-N., & Maher, N. (2024). Sea ice feedbacks cause more greenhouse cooling than greenhouse warming at high northern latitudes on multi-century timescales. *Environmental Research: Climate*, *3*(4), 041003. https://doi.org/10.1088/2752-5295/ad8026

Krasting, J., Dunne, J., Shevliakova, E., & Stouffer, R. (2014). Trajectory sensitivity of the transient climate response to cumulative carbon emissions. *Geophysical Research Letters*, *41*(7), 2520–2527. https://doi.org/10.1002/2013gl059141

Lee, Y.-C., Liu, W., Fedorov, A. V., Feldl, N., & Taylor, P. C. (2024). Impacts of Atlantic meridional overturning circulation weakening on arctic amplification. *Proceedings of the National Academy of Sciences*, *121*(39), e2402322121. https://doi.org/10.1073/pnas.2402322121

Liang, Y.-C., Polvani, L. M., & Mitevski, I. (2022). Arctic amplification, and its seasonal migration, over a wide range of abrupt CO_2 forcing. *npj Climate and Atmospheric Science*, *5*(1), 14. https://doi.org/10.1038/s41612-022-00228-8

Manabe, S., & Stouffer, R. J. (1980). Sensitivity of a global climate model to an increase of CO_2 concentration in the atmosphere. *Journal of Geophysical Research*, *85*(C10), 5529–5554. https://doi.org/10.1029/jc085ic10p05529

Manabe, S., & Wetherald, R. T. (1975). The effects of doubling the CO_2 concentration on the climate of a general circulation model. *Journal of the Atmospheric Sciences*, *32*(1), 3–15. https://doi.org/10.1175/1520-0469(1975)032<0003:teodtc>2.0.co;2

Marshall, J., Scott, J. R., Armour, K. C., Campin, J.-M., Kelley, M., & Romanou, A. (2015). The ocean's role in the transient response of climate to abrupt greenhouse gas forcing. *Climate Dynamics*, *44*(7–8), 2287–2299. https://doi.org/10.1007/s00382-014-2308-0

Merlis, T. M., & Henry, M. (2018). Simple estimates of polar amplification in moist diffusive energy balance models. *Journal of Climate*, *31*(15), 5811–5824. https://doi.org/10.1175/jcli-d-17-0578.1

Mitevski, I., Orbe, C., Chemke, R., Nazarenko, L., & Polvani, L. M. (2021). Non-monotonic response of the climate system to abrupt CO_2 forcing. *Geophysical Research Letters*, *48*(6), e2020GL090861. https://doi.org/10.1029/2020gl090861

Mitevski, I., Polvani, L. M., He, H., Vecchi, G. A., Orbe, C., Soden, B. J., & Miller, R. L. (2025). State dependence of CO_2 effective radiative forcing from 1/16× to 16× CO_2. *Journal of Climate*, *38*(19), 5323–5333. https://doi.org/10.1175/jcli-d-24-0387.1

Pedro, J., Martin, T., Steig, E., Jochum, M., Park, W., & Rasmussen, S. (2016). Southern ocean deep convection as a driver of Antarctic warming events. *Geophysical Research Letters*, *43*(5), 2192–2199. https://doi.org/10.1002/2016gl067861

Pedro, J. B., Jochum, M., Buizert, C., He, F., Barker, S., & Rasmussen, S. O. (2018). Beyond the bipolar seesaw: Toward a process understanding of interhemispheric coupling. *Quaternary Science Reviews*, *192*, 27–46. https://doi.org/10.1016/j.quascirev.2018.05.005

Pendergrass, A. G., Conley, A., & Vitt, F. M. (2018). Surface and top-of-atmosphere radiative feedback kernels for CESM-CAM5. *Earth System Science Data*, *10*(1), 317–324. https://doi.org/10.5194/essd-10-317-2018

Pithan, F., & Mauritsen, T. (2014). Arctic amplification dominated by temperature feedbacks in contemporary climate models. *Nature Geoscience*, *7*(3), 181–184. https://doi.org/10.1038/ngeo2071

Previdi, M., Janoski, T. P., Chiodo, G., Smith, K. L., & Polvani, L. M. (2020). Arctic amplification: A rapid response to radiative forcing. *Geophysical Research Letters*, *47*(17), e2020GL089933. https://doi.org/10.1029/2020gl089933

Rantanen, M., Karpechko, A. Y., Lipponen, A., Nordling, K., Hyvärinen, O., Ruosteenoja, K., et al. (2022). The arctic has warmed nearly four times faster than the globe since 1979. *Communications Earth & Environment*, *3*(1), 168. https://doi.org/10.1038/s43247-022-00498-3

Roe, G. H., Feldl, N., Armour, K. C., Hwang, Y.-T., & Frierson, D. M. (2015). The remote impacts of climate feedbacks on regional climate predictability. *Nature Geoscience*, *8*(2), 135–139. https://doi.org/10.1038/ngeo2346

Rugenstein, M., Bloch-Johnson, J., Abe-Ouchi, A., Andrews, T., Beyerle, U., Cao, L., et al. (2019). Longrunmip: Motivation and design for a large collection of millennial-length AOGCM simulations. *Bulletin of the American Meteorological Society*, *100*(12), 2551–2570. https://doi.org/10.1175/bams-d-19-0068.1

Salzmann, M. (2017). The polar amplification asymmetry: Role of Antarctic surface height. *Earth System Dynamics*, *8*(2), 323–336. https://doi.org/10.5194/esd-8-323-2017

Screen, J. A., & Simmonds, I. (2010). The central role of diminishing sea ice in recent arctic temperature amplification. *Nature*, *464*(7293), 1334–1337. https://doi.org/10.1038/nature09051

Serreze, M. C., Barrett, A., Stroeve, J., Kindig, D., & Holland, M. (2009). The emergence of surface-based arctic amplification. *The Cryosphere*, *3*(1), 11–19. https://doi.org/10.5194/tc-3-11-2009

Shell, K. M., Kiehl, J. T., & Shields, C. A. (2008). Using the radiative kernel technique to calculate climate feedbacks in NCAR's Community Atmospheric Model. *Journal of Climate*, *21*(10), 2269–2282. https://doi.org/10.1175/2007jcli2044.1

Shields, C. A., Bailey, D. A., Danabasoglu, G., Jochum, M., Kiehl, J. T., Levis, S., & Park, S. (2012). The low-resolution CCSM4. *Journal of Climate*, *25*(12), 3993–4014. https://doi.org/10.1175/jcli-d-11-00260.1

Soden, B. J., Held, I. M., Colman, R., Shell, K. M., Kiehl, J. T., & Shields, C. A. (2008). Quantifying climate feedbacks using radiative kernels. *Journal of Climate*, *21*(14), 3504–3520. https://doi.org/10.1175/2007jcli2110.1

Stocker, T. F., & Schmittner, A. (1997). Influence of CO_2 emission rates on the stability of the thermohaline circulation. *Nature*, *388*(6645), 862–865. https://doi.org/10.1038/42224

Stouffer, R. J., & Manabe, S. (1999). Response of a coupled ocean–atmosphere model to increasing atmospheric carbon dioxide: Sensitivity to the rate of increase. *Journal of Climate*, *12*(8), 2224–2237. https://doi.org/10.1175/1520-0442(1999)012<2224:roacoa>2.0.co;2

Stuecker, M. F., Bitz, C. M., Armour, K. C., Proistosescu, C., Kang, S. M., Xie, S.-P., et al. (2018). Polar amplification dominated by local forcing and feedbacks. *Nature Climate Change*, *8*(12), 1076–1081. https://doi.org/10.1038/s41558-018-0339-y

Sweeney, A. J., Fu, Q., Po-Chedley, S., Wang, H., & Wang, M. (2023). Internal variability increased arctic amplification during 1980–2022. *Geophysical Research Letters*, *50*(24), e2023GL106060. https://doi.org/10.1029/2023gl106060

Winton, M. (2006). Amplified arctic climate change: What does surface albedo feedback have to do with it? *Geophysical Research Letters*, *33*(3). https://doi.org/10.1029/2005gl025244

References From the Supporting Information

Meinshausen, M., Smith, S. J., Calvin, K., Daniel, J. S., Kainuma, M. L., Lamarque, J.-F., et al. (2011). The rcp greenhouse gas concentrations and their extensions from 1765 to 2300. *Climatic Change*, *109*(1), 213–241. https://doi.org/10.1007/s10584-011-0156-z